



HAL
open science

Numerical modelling of parts distortion and beam supports breakage during selective laser melting (SLM) additive manufacturing

Yves Bresson, Amèvi Tongne, Pierre Selva, Lionel Arnaud

► **To cite this version:**

Yves Bresson, Amèvi Tongne, Pierre Selva, Lionel Arnaud. Numerical modelling of parts distortion and beam supports breakage during selective laser melting (SLM) additive manufacturing. The International Journal of Advanced Manufacturing Technology, 2022, 119, pp.5727-5742. 10.1007/s00170-021-08501-5 . hal-04488952

HAL Id: hal-04488952

<https://hal.science/hal-04488952v1>

Submitted on 4 Mar 2024

HAL is a multi-disciplinary open access archive for the deposit and dissemination of scientific research documents, whether they are published or not. The documents may come from teaching and research institutions in France or abroad, or from public or private research centers.

L'archive ouverte pluridisciplinaire **HAL**, est destinée au dépôt et à la diffusion de documents scientifiques de niveau recherche, publiés ou non, émanant des établissements d'enseignement et de recherche français ou étrangers, des laboratoires publics ou privés.







OATAO is an open access repository that collects the work of Toulouse researchers and makes it freely available over the web where possible

This is an author's version published in: <http://oatao.univ-toulouse.fr/28748>

Official URL:

<https://doi.org/10.1007%2Fs00170-021-08501-5>

To cite this version:

Bresson, Yves  and Tongne, Amèvi  and Selva, Pierre  and Arnaud, Lionel  *Numerical modelling of parts distortion and beam supports breakage during selective laser melting (SLM) additive manufacturing*. (2022) *The International Journal of Advanced Manufacturing Technology*. ISSN 2252-0406

Any correspondence concerning this service should be sent to the repository administrator: tech-oatao@listes-diff.inp-toulouse.fr

Numerical modelling of parts distortion and beam supports breakage during selective laser melting (SLM) additive manufacturing

Yves Bresson^{1,2} · Amèvi Tongne¹ · Pierre Selva¹ · Lionel Arnaud¹

Abstract

The Selective Laser Melting (SLM) process has been progressively endorsed as an industrial manufacturing technique to produce high value-added components. However, one of the main obstacles to its wide application is the uncertainty regarding the successful completion of the manufacturing process. Mechanical stresses are generated and accumulated during the process, which may lead to the parts warping and cracking. Support structures may also detach from the part but it is not certain that these cracks conduct to the manufacturing failure. The process simulations currently available do not consider the cracking of the supports and the ongoing part's deflection. The aim of this study is to investigate cone supports fracture behaviour comparing the results from a numerical model and the manufacturing of an industrial part. A model using 1D-beam elements to mesh the supports has been developed to consider the damage of the supports, their breakage and the ongoing deflection. Some numerical convergence issues are identified and solutions are proposed. Specific experimental set-ups are developed to characterise the behaviour of the supports individually and as a group. Significant improvements are denoted while injecting the measured characteristics within the model. Some key parameters of the supports damage behaviour are identified. It is shown that the supports mechanical characteristics are significantly different from the parts due to their manufacturing conditions and environment. Also, limitations regarding the characterisation of the supports as well as strong numerical convergence issues brought by multiple supports cracking are discussed.

Keywords Additive manufacturing · SLM · Numerical simulation · Beam supports · Breakage · Stainless steel (316L)

Highlights

- Finite element modelling of cone supports and specifically the teeth area.
- Support breakage simulation and part's distortion after supports breakages.
- Model results are compared to four additive manufacturing commercial software.

✉ Yves Bresson
yves.bresson@enit.fr

Amèvi Tongne
amevi.tongne@enit.fr

Pierre Selva
pierre.selva@enit.fr

Lionel Arnaud
lionel.arnaud@enit.fr

¹ Laboratoire Génie de Production, INP-ENIT, 47 Avenue d'Azereix, Tarbes 65000, France

² Halbronn, Z.I. Lognes, rue des Campanules, Marne-La-Vallée 77437, France

1 Introduction

Additive manufacturing (AM) denotes a group of manufacturing processes that permits complex near net shape components. Selective Laser Melting (SLM) is one of the most common metal AM techniques used in the industry. It consists of spreading thin powder layers (30 - 70 μm thick) over a build plate, then consecutively scan and melt the powder using a high-power laser heat source under a protective atmosphere.

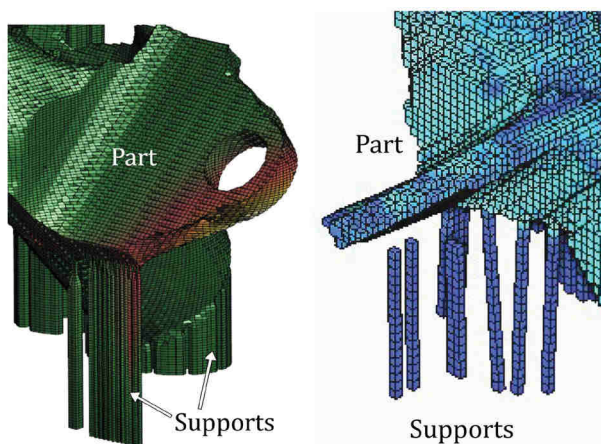
An important characteristic of SLM process is its requiring of supports anchoring the parts to the build plate surface [1]. Supports used during the process have three main functions [2, 3]:

- Anchoring the over-hanged surfaces to the build plate.
- Reducing part's distortion.
- Conducting heat away from the upper material.

Since supports manufacturing requires scanning time, post-processing steps and consumes material, it generates non-negligible costs [4]. A recent machine manufacturer [5] and a few studies have been focusing on ways to avoid or to minimize their usage [6, 7] and the mechanical post-processing steps [8–12].

Supports are to be present in sufficient amount on overhanging regions, namely those inclined with an angle below 45° with the horizontal plane [13, 14]. Numerous supports geometries could be used. Most of them are presented in the works conducted by Jiang [3], Calignano [13] and Leary [15]. This study will focus on beam-like (also named cone or strut-like) supports, commonly used in the industry. In addition, standard process parameters optimized for this class of supports have been used, provided by the machine manufacturer.

Supports could help prevent the occurring of parts deformation, warping and cracking [16], which are part of the main four SLM defect types (including porosity [17]). Several commercial codes are conceived to grant the deformation and residual stress distributions along with the manufactured parts. Some of them (Inspire [18], Amphyon [19], Netfabb [20], Simufact [21], ESI Additive Manufacturing [22]) have been tested in this article on an industrial part. The various models are based on different approaches (such as 3D-modelling, homogenised structures, plate elements, etc.) and most of them precisely model the supports and their distortion, as illustrated in Fig. 1. However, none of these software is able to model the supports breakage and the continuation of manufacturing with fractured supports. Detached Netfabb supports on Fig. 1 are not detached from a computed fracture: it is due to a display error caused by the meshing.



(a) Amphyon's support meshing (b) Netfabb's support distortion results.

Fig. 1 Examples of support meshing from two commercial codes

It is commonly accepted that the damage of the supporting structure generally leads to failure of the part's manufacturing. However, the cone supports' fracture in a dense tree-like structure could happen on multiple occasions without degrading the part. This article aims to simulate the damage and fracture of the supports used in additive manufacturing and to evaluate the final result.

The numerical model developed in this work predicts supports fracture using beam elements and voxel elements to mesh supports and parts. Thus, the article is decomposed as follows: Section 2 refers to the literature regarding both the modelling and optimisation processes in SLM with a specific focus on supports. In Section 3, a practical industrial case is presented and simulated using current commercial codes. Distortion results regarding the supports and the narrowing area at the interface with the part are discussed. In Section 4, a novel modelling approach for cone supports is presented using one-dimensional beam elements in Finite Element (FE) analysis. Numerical results and parameters are discussed in Section 5.

2 State of the art

2.1 SLM general modelling methods

Considering SLM process numerical modelling, several spatial and temporal discrete levels could be used and even combined in multiscale frameworks [23–25]. The work presented in this article concentrates solely on modelling part-scale deformations developed during the process.

As discussed by [26–28], thermal distortions and residual stresses are consequences of the process complex thermal history. The SLM process involves extremely fast cooling / heating phases that could reach magnitudes in the order of $10\text{ K}/\mu\text{s}$ to $20\text{ K}/\mu\text{s}$ [29]. Hence, numerous studies have developed sophisticated thermomechanical models to capture the impacts of those thermal loadings on mechanical residual stresses and deformations [30–35]. Several numerical methods, such as quiet elements method or inactive elements method, could be used to model the SLM process, as described by [36]. Michaleris [37] mixed these approaches in a hybrid quiet inactive element method to mitigate each method's drawbacks. Moreover, whereas the physical layer thickness ranges in the order of tens of microns, it is a common approach to model thicker layers (macro layers) to reduce computational times [38]. Hence, in the numerical modelling process, it is possible to activate the elements one by one, in a layer-wise fashion, or macro layer by macro layer.

A method first developed for the welding process in the 70s is referred to as the inherent strain method [39]. This method allows a significant reduction of the computational

effort. Numerous works have used such methods to simulate metal AM processes, based on the inherent strain approach: some of them advanced limitations and others proposed some improvements [40–44]. These inherent strain-based methods are used in recent studies which simulate and even optimise the supports used in SLM [45–48].

2.2 Support modelling approaches

The connection area between supports and parts (the teeth) often need to be optimised [49]. It could be modeled by a very thin mesh size to represent the residual stresses finely at these locations. For instance, Cao et al. [8, 50] have been using almost 200 000 brick-type elements to simulate the machining process of a few beam supports.

Also, since the supports' scanning strategies and geometries are different from the parts, it is assumed that the support material properties might vary. Thus, some studies have been considering tensile testing supports of different geometries [15, 16, 51] to characterise their behaviour. However, there is still a lack of data that could help AM-engineers to design supports, and standard methods to test these structures repetitively are still required.

2.3 Supports design and optimisation

Well-developed AM process studies can also be found in patents. Many provide methods regarding supports such as their positioning [52–54], their geometry [53, 55–64], methods to break them easily [65] or to design them in an effective heat diffusion fashion [66, 67]. Numerous parameters have an impact on supports integrity, such as scanning parameters [7, 68, 69] and parts orientations [6, 70, 71]. Some supports optimization researches [72–74] showed that the ability of the supports to diffuse heat out from upper layers could improve parts overall fatigue performance [75]. Several studies have focused on comparing and selecting geometries based on objective function or experimental testing [2, 13, 17, 49, 76]. Recent works have designed supports using topological optimization [45, 48, 77] and taking into account supports crack risk during manufacturing [47, 78].

Hence, supports are the subject of numerous research since the last decade, and there is still a lack of understanding regarding their behaviour during the process. In particular, several research works have developed optimization frameworks regarding the supports geometries and weight reduction. But a few tried to anticipate the supports breakage and the subsequent part distortion [79]. It is common that a few supports break away from the part without ceasing the build or invalidating the part, especially because the supports breakage would generally happen while scanning a layer far above the fracture site, or even during the final cool down of the build.

3 Study case

3.1 Description

The part used in this study is a hydraulic joint used in the aeronautic field to channel oil fluids into aircraft components. The part has been topologically optimised, taking into account all lifetime forces, including machining forces, in a previous work [80]. The topological optimization led to a weight reduction from 210 g to less than a 100 g and 75% hydraulic performance improvements. The initial and final geometries are shown in Fig. 2. Only one part has been placed on the build plate, and its supporting can be seen in Fig. 2c. Its orientation has been chosen mainly to avoid the use of internal supports within the oil pipes. The beam supports geometries as well as their positioning are user-defined. The total manufacturing height was 66.8 mm.

Several Additive Manufacturing machines and materials have been tested to manufacture the hydraulic joint. The same observation was made with every configuration: the supports broke under the hydraulic joint arm. The resulting manufacturing using a Renishaw AM 400 machine is displayed in Fig. 3. The machine used a 400 W fiber laser source of 70 μm beam diameter. The material used was 316 L stainless steel powder provided by the machine manufacturer

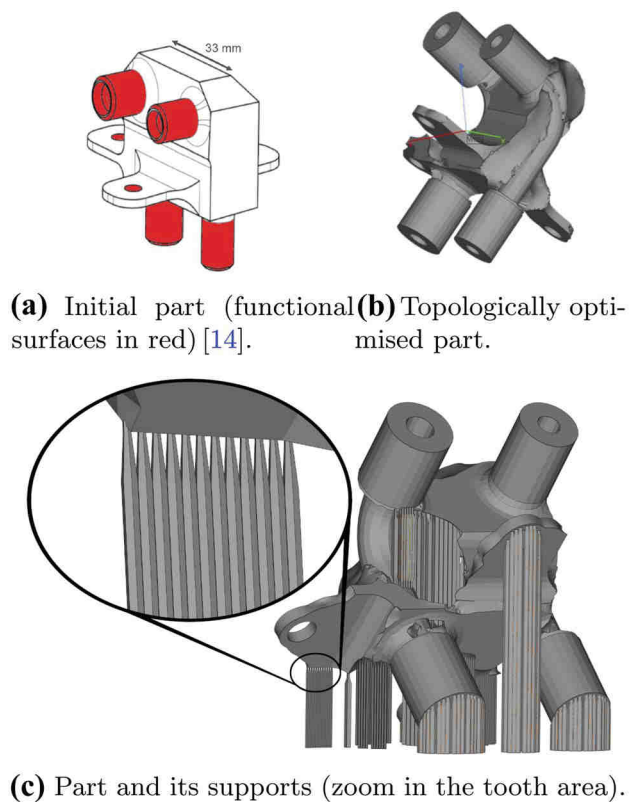


Fig. 2 Industrial hydraulic joint [80]

Table 1 316L stainless steel powder characteristics

Elements	Fe	Cr	Ni	Mo	Mn	Si	N	O	P	C	S
Mass (%)	Bal.	16 – 18	10 – 14	2 – 3	≤ 2	≤ 1	≤ 0.1	≤ 0.1	≤ 0.045	≤ 0.03	≤ 0.03

(particle size of 15-45 μm , the chemical composition from the provider [81] is detailed in Table 1). The standard manufacturing process parameters are listed in Table 2.

The manufacturing process has been considered successful, however 12 supports located under the arm of the hydraulic joint had broken, as shown in Fig. 3. Supports detachment caused the part to warp a little and to collide smoothly with the layering system, even though the manufacturing process completed. While the precise instant of the rupture cannot be defined precisely, it is assumed that the smooth collision occurred hundreds of layers above the supports. It could be explained by the cumulative thermal shrinkage effect during the build up of the component. The shrinkage of later printed layers results in an additional stress of the layers below. This, in turn, would lead to supports breakage when exceeding their ultimate tensile stress.

For availability reasons, all the mechanical samples used for the characterization process were manufactured with a DMP ProX300 machine. The machine parameters are displayed in Table 2.

3.2 Numerical simulation using commercial codes

The above-mentioned additively manufactured part has been simulated using four commercial codes: Netfabb, Amphyon, Inspire and ESI Additive Manufacturing. Due to the specificity of each software, it was not possible to compare the simulation results using the same meshing strategy or the same computation time. Hence, these simulations were not meant to quantitatively compare the software, but to illustrate obtained results from each of these

Table 2 SLM process parameters for 316L stainless steel material. No contour parameter is set on ProX300 machine

Parameter	AM400	ProX300
Layer thickness	50 μm	40 μm
Beam diameter	70 μm	70 μm
Preheating temperature	170° C	–
Bulk part		
Laser power	195 W	172 W
Scanning speed	750 mm/s	1800 mm/s
Cone supports		
Laser power	195 W	172 W
Scanning speed	750 mm/s	1800 mm/s
Contours		
Laser power	110 W	–
Scanning speed	200 mm/s	–

commercial code currently available. The global results of each software are displayed in Table 3.

The deformation results are illustrated in Fig. 4. They range from 0.40 mm to 2.52 mm. Each code predicted high deformation magnitudes in the area where the supports experimentally broke away. Only Amphyon software could finely mesh the supports.

Hence, several AM software are able to simulate the parts distortion. Most of them predict accurately the defects location and the global deformation as well as local plasticity. However, none of them model the supports damage or their breakage, which is an important consideration to prevent the whole build interruption.

4 The numerical models developed and the experimental data used

4.1 Numerical method

The numerical model consisted of an assembly of several instances: a build plate, the supports, and the hydraulic joint (the part). The build plate was a rectangular instance

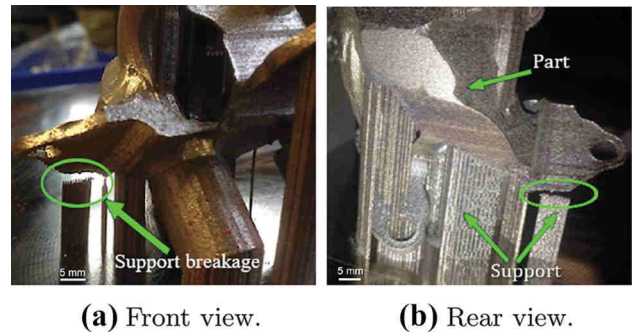


Fig. 3 Distortion of the part causing supports breakage

Table 3 Commercial codes hydraulic block simulation results. “NC” stands for “Not Communicated” information by the software provider

Code	Max displacement	Non cubic voxels	Computation time
Amphyon	1.75 mm	Yes	<10 min.
Netfabb	2.53 mm	No	NC
Inspire	0.68 mm	No	<10 min.
ESI	2.17 mm	No	NC

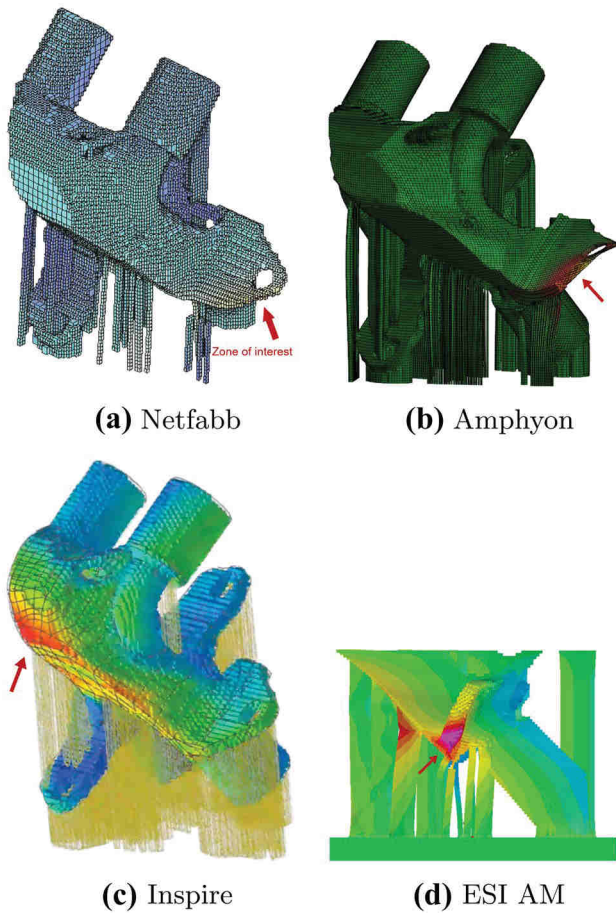
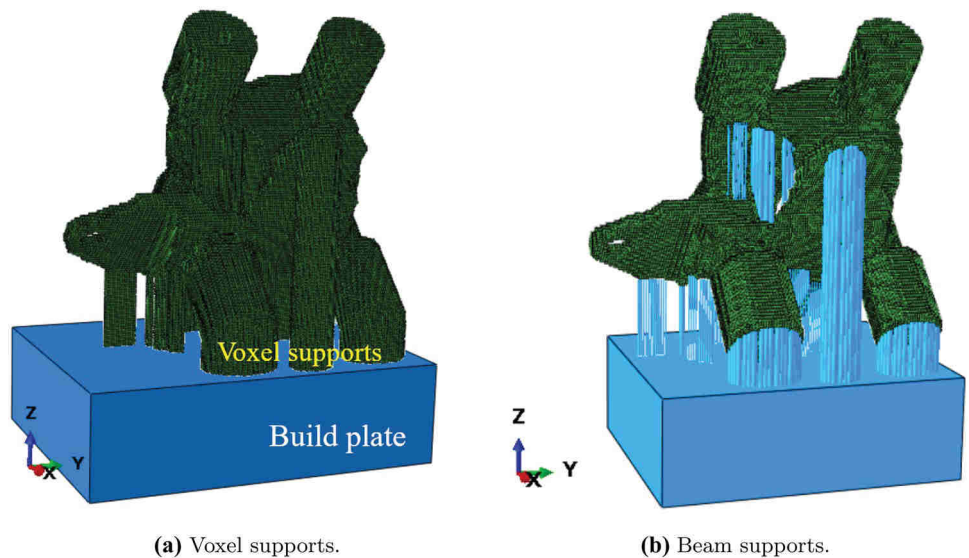


Fig. 4 Four commercial codes hydraulic block simulation displacement fields, zoom on the hydraulic joint arm. Simulated critical regions are indicated with a red arrow

of dimensions 70.9 mm×53.9,mm×20,mm meshed with 153 360 Abaqus C3D8-type (brick) elements. The hydraulic joint was meshed using cubic voxel elements before being

Fig. 5 joint Abaqus models with the build plate, voxel and beam (b) supports



imported in ABAQUS software: 203 736 C3D8-type voxel elements were used.

The model was developed using Abaqus/standard, and the model generation was fully automated using a python script. The resolution was fully mechanical: user-defined thermal strains were applied by incrementally varying the temperature fields. Using a linear Coefficient of Thermal Expansion (CTE), these temperature variations drove thermal-induced strains. In this study, the CTE value was set to $18 K^{-1}$ [82]. The part's mesh size was set to 0.5 mm, which corresponds to the thickness of ten physical layers. This layers bundling will be mentioned as a *macro layer* in the next sections. The first simulation step in Abaqus consisted of deactivating the hydraulic joint and the supports. Then, at each further step, a novel macro layer was activated at the material melting temperature (1673 K). To simplify the study, no thermal equation was solved: the cooling process was simulated by setting consecutive temperature drop steps. Hence, at each step, each already activated macro layer was cooled by 153 K until it reaches the room-ambient temperature. Numerical thermal studies indicated that nine steps were required for the layer temperature to reach the room-ambient temperature (293 K).

Two models were created with different meshing strategies for the supports:

The first model employed 0.5 mm length Abaqus C3D8-type voxel elements (see Fig. 5a) to mesh the supports. This way, 47 857 elements were added to model the support structures. The voxels could not represent the narrowing at the zone linking the supports to the part (the tooth area). Section and material properties were homogeneous throughout the supports. This is due to the difficulty of identifying the voxels corresponding to the supports teeth, which are merged with the supports core and the part while using such mesh length.

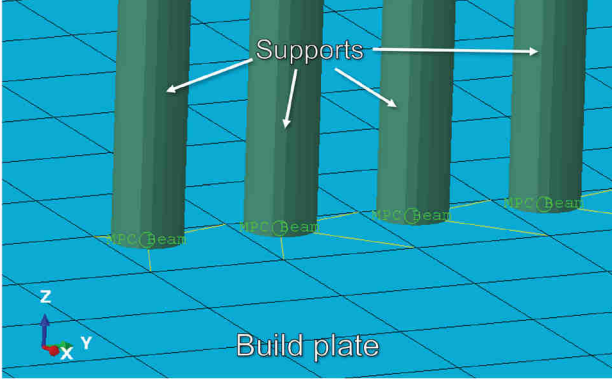


Fig. 6 MPC constraints between some supports and the build plate

The second model consisted of meshing the supports with Abaqus B31-type beam elements (see Fig. 5b). Multi-Point Constraints (MPC) are used to connect the supports' ends to the build plate and the hydraulic joint (see Figs. 6 and 7). Although the voxel elements could not represent the geometrical narrowing at the tooth area, 1D elements have been implemented with a uniformly reduced section to model the narrowing at the tooth area. It is the scope of future studies to use progressive section reduction at these locations instead of a uniformly reduced section.

Regarding the mechanical properties, literature values were used since 316L material mechanical characteristics have been well studied for the SLM process. Mean values from literature are listed in Table 4 [83–95]. Since the thermal history is not computed in this study (the model is fully mechanical), the material parameters are temperature-independent. This behavior could be improved in a future study, specifically, the temporal aspect is not considered (to introduce the viscoplasticity for instance). It can be seen from Table 4 that the fracture strain $A\%$ parameter taken from the average literature values is less than the standard specified value [96]. It can be explained by the fact that the standard value was set for conventional annealed and cold-worked austenitic stainless steels, although the literature values were measured as-built from SLM specimens. Hence, it is expected that the as-built SLM-manufactured specimens are more fragile than conventional 316L.

To model the overlapping at the base of the supports, horizontal 1D elements have been added all along the vertical cone supports, binding the cone supports to one another. Supports are generally linked to their neighbours at the base, hence the overlapping should be considered. Specifically, the horizontal stiffness resulting from the overlapping should be accounted for. Several investigations were launched and promising results were obtained on simple models. However, using the hydraulic joint model, too many supplementary instances and elements were generated, and the automatic scripts could not complete. An alternative way will be

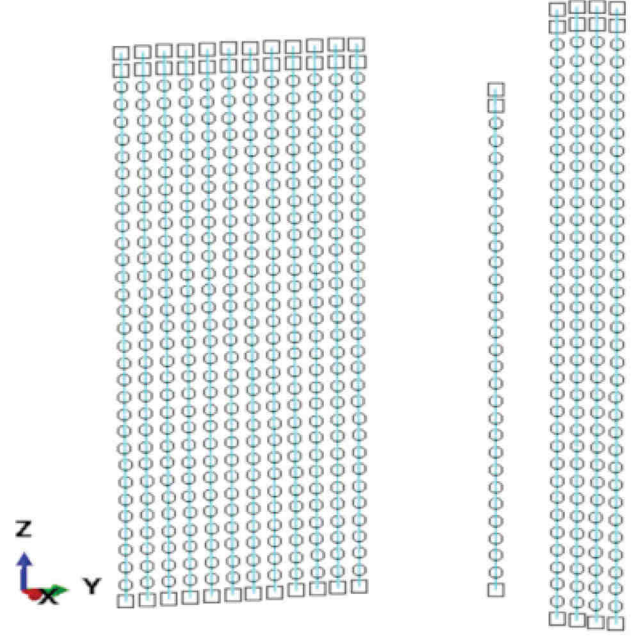


Fig. 7 1D Beam supports nodes

investigated as an improvement to account for the overlapping at the base of the cone supports.

A ductile damage initiation criterion [97] was defined for predicting the onset of damage in every models. Its value corresponded to the fracture strain (34%) mentioned in Table 4. A displacement damage evolution was used to link the damage as a function of the plastic displacement after damage initiation. The damage varied linearly with the deformation (*Linear Softening* in Abaqus). The effective plastic displacement at the point of failure parameter \bar{u}_f^{pl} [98] was set to 0.05 mm for an element length of 0.5 mm. This parameter is linked to the element damage variable \dot{d} as [98] :

$$\dot{d} = \frac{L \dot{\epsilon}^{pl}}{\bar{u}_f^{pl}} \quad (1)$$

where L is the characteristic length of the element (equal for all elements throughout the model) and $\dot{\epsilon}^{pl}$ is the equivalent plastic strain variable.

Table 4 Mean 316L stainless steel mechanical properties from [83–95] and ASTM A666-15 Standard [96]

Characteristics	Literature	ASTM Standard
Young Modulus E	180GPa	-
Yield strength R_e	496MPa	170 MPa
Tensile strength R_m	614MPa	485 MPa
Fracture strain $A\%$	34%	40%

Then, when $L \dot{\epsilon}^{pl}$ equals \bar{u}_f^{pl} value, the degradation is completed. Elements are deleted from the simulation once the damage variable is equal to 1. These damage parameters were kept constant for all element sizes presented in the following sections.

Using beam elements to mesh the supports has generated numerous instabilities, and convergence issues came out. It was determined that the instabilities come mainly from the buckling phenomena using an elasto-plastic behaviour : Indeed, some supports are under compression loading. The Abaqus standard solver used in this model is not able to overcome such instabilities occurring at the same time on various locations, so the solver would not converge. Two strategies have been tested to tackle these problems in a static resolution : using another resolution algorithm or using simplifying hypotheses to prevent the buckling phenomenon. Some tests have been done and showed that the Abaqus Riks solver was able to converge for a single beam in compression while using elasto-plastic material properties. However, the *Activation* tool is not available using this solver and mixing both standard Static and Riks solvers would require to restart the computations at each step. This solution is not recommended because of the computation efforts required.

The second strategy prevents all the rotations at each node of the beam. This strong assumption artificially stiffens the structure but it is expected from experimental trials that the main damage come from traction loadings at the tooth area. This assumption will be used in the following models.

4.2 Numerical results and experimental comparison

4.2.1 3D-voxel and 1D-beam elements simulation results

Von Mises stress and displacement fields using 0.5 mm voxel elements to mesh the supports are displayed in Fig. 8. No supports were detached from the part using voxel elements (as seen in Fig. 8c), however the maximum displacement value (2.05 mm) is significant and would lead to invalidate the part. It can also be seen from Fig. 8a that some excessive stress values were obtained. All these excessive values (significantly higher than the tensile strength of 614 MPa, mentioned in Table 4) are due to the large mesh size. Indeed, the stresses are computed at the elements integration points, however, the contouring algorithm used by Abaqus to fill the contour plot (i.e. the stress fields) makes use of the nodal values. The nodal values are then extrapolated from the integration points values [99]. In fact, while extracting the von Mises stress values at the integration points of the hydraulic joint elements, the value did not exceed 614 MPa.

The stress levels of interest are those of the supports, shown in the black frame in Fig. 8c in the range 0 – 614 MPa

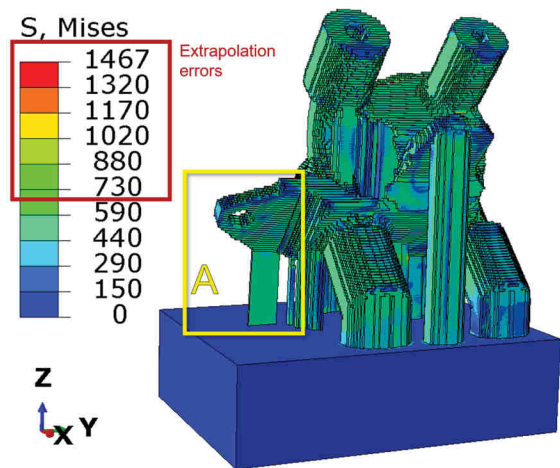
(see Table 4). It could be noted that the stress distribution within the voxel supports looks homogeneous. The global displacement fields are displayed in Fig. 8b and the maximum displacement values are located at the hydraulic joint arm, as shown in Fig. 8d. It corresponds to the location of the supports breakages and significant distortion of the manufactured part. The observed part rotation happened after the fracture of numerous supports, hence it was not considered. The computation time for this simulation is about 1.6 day using 12 core AMD Opteron™ 6376 2.3 GHz – 128 Gb RAM (Random Access Memory).

Simulation results using beam elements to mesh the 354 supports are displayed on Fig. 9.

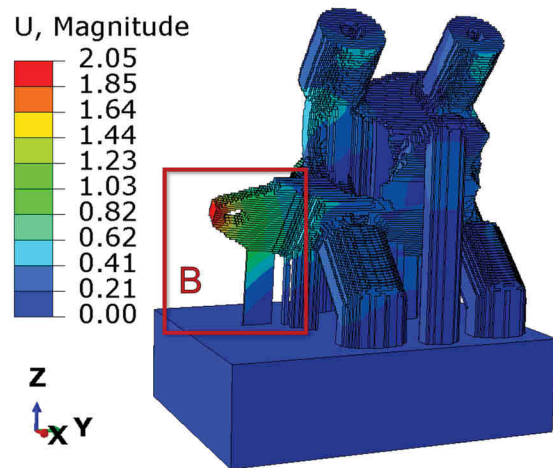
The computation times for this model were about 1.8 day on 12 core AMD Opteron™ 6376 2.3 GHz – 128 Gb RAM. Figures 9a and 9b display the whole Abaqus assembly, with *render beam profile* option activated (this option would show the 1D-beam elements with a 3D profile, as in Fig. 5b). Figure 9c and d display the supports only, also with *render beam profile* deactivated. Unlike the voxel supports, the 1D cone supports stress fields are not homogeneous through the supports for several reasons : the main stress values are located at the teeth area while using the 1D-beam elements since the section reduction is considered. Also, in this case, each beam is independent from its beam neighbours, contrarily to the voxels, connected one to the others. Just like the voxel model, excessive stress values were artificially extrapolated by Abaqus at some part elements. However, the stress range within the supports does not exceed the tensile strength from Table 4. Despite the fact that the two models integrate damage and fracture, only beam supports have been detached from the part during the simulation. The detached support elements are those for which the damage was completed and they were deleted during the simulation. There are 126 deleted elements, hence 126 detached supports. This number of detached supports is significantly higher than the experimental production (supports breakages were located on the hydraulic joint arm as shown in Fig. 3).

It could also be noticed that all the breakages appeared at the tooth location, no supports have been detached from the build plate or at a midsection. This behaviour is due to the radius shrinkage at the tooth area which results in a stress concentration area. It is worth mentioning that some supports have completed the damage and their teeth has been detached while suffering compression solicitations. This behaviour is not representative since the cracks may not propagate as they could in traction. These compression loadings are the reason for hindering all the rotations, they lead to buckling phenomena and convergence issues.

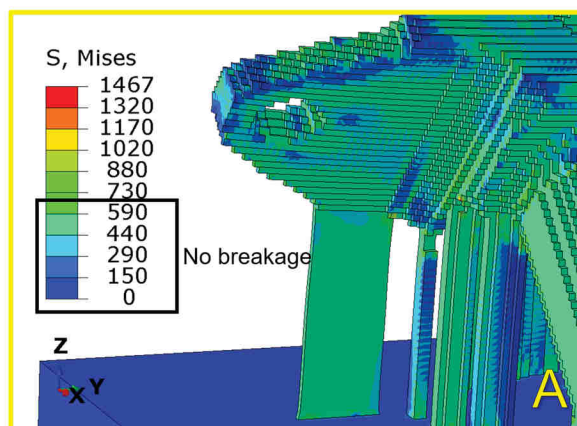
The simulated displacement magnitude (maximum value of 2.94 mm) and the number of detached supports is too large compared to the experimental results (12 supports



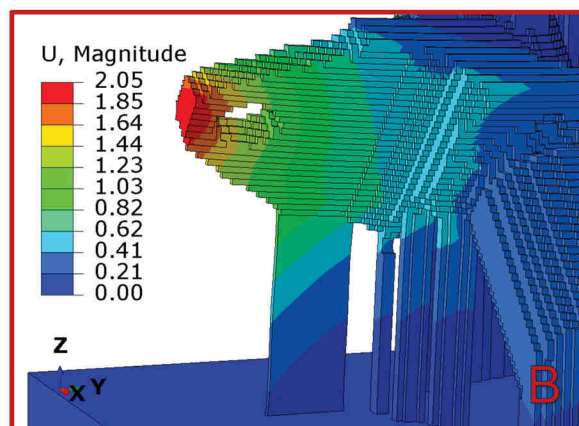
(a) Von Mises stress fields (MPa).



(b) Displacement fields (mm).



(c) Von Mises stress (MPa), zoom on supports and hydraulic joint arm.



(d) Displacement fields (mm), zoom on supports and hydraulic joint arm.

Fig. 8 3D-voxel simulation results: stress and displacement fields

instead of the 126 detached supports in the simulation). It is necessary to understand the reasons of such discrepancy and to calibrate the model to fit the actual supports behaviour. Hence, in the next sections, some investigations will be launched to identify the main parameters within the model that generate such differences in the simulation results. First, we will look at the mechanical behaviour of the supports as a group, in a controlled loading case. Hence, a self-developed multi-support set up will be tensile tested and the force-displacement measurements will be compared to a numerical simulation.

4.2.2 Multi-supports set up results

The previous 1D-beam elements supports model have converged and some of the beam supports detached from the part, including those at the arm of the hydraulic joint (the location we expect from the experimental results shown in

Fig. 3). However, too many beams have been detached from the part and it may be due to numerous factors (i.e. too weak material properties, non-representative temperature conditions, abrupt section reduction for teeth radius, bending phenomenon in the supports, stiffening from the neighbourhood supports, damage during compression phase, etc.). At first, we will compare the behaviour of an experimental set up having several cone supports with a tensile test at room temperature and compare the results with a simulation. The same parameters as in the previous models will be used.

A multi-supports set up (shown in Fig. 10) is additively manufactured for tensile testing. Its objective is to compare the maximum force applied to detach the beam supports from a part, experimentally and numerically, using literature material properties. Seventy-nine supports of base diameter 1.10 mm were meshed with B31 beam elements, their teeth having a uniform diameter of 0.75 mm (the minimum diameter of the real teeth). The section variation

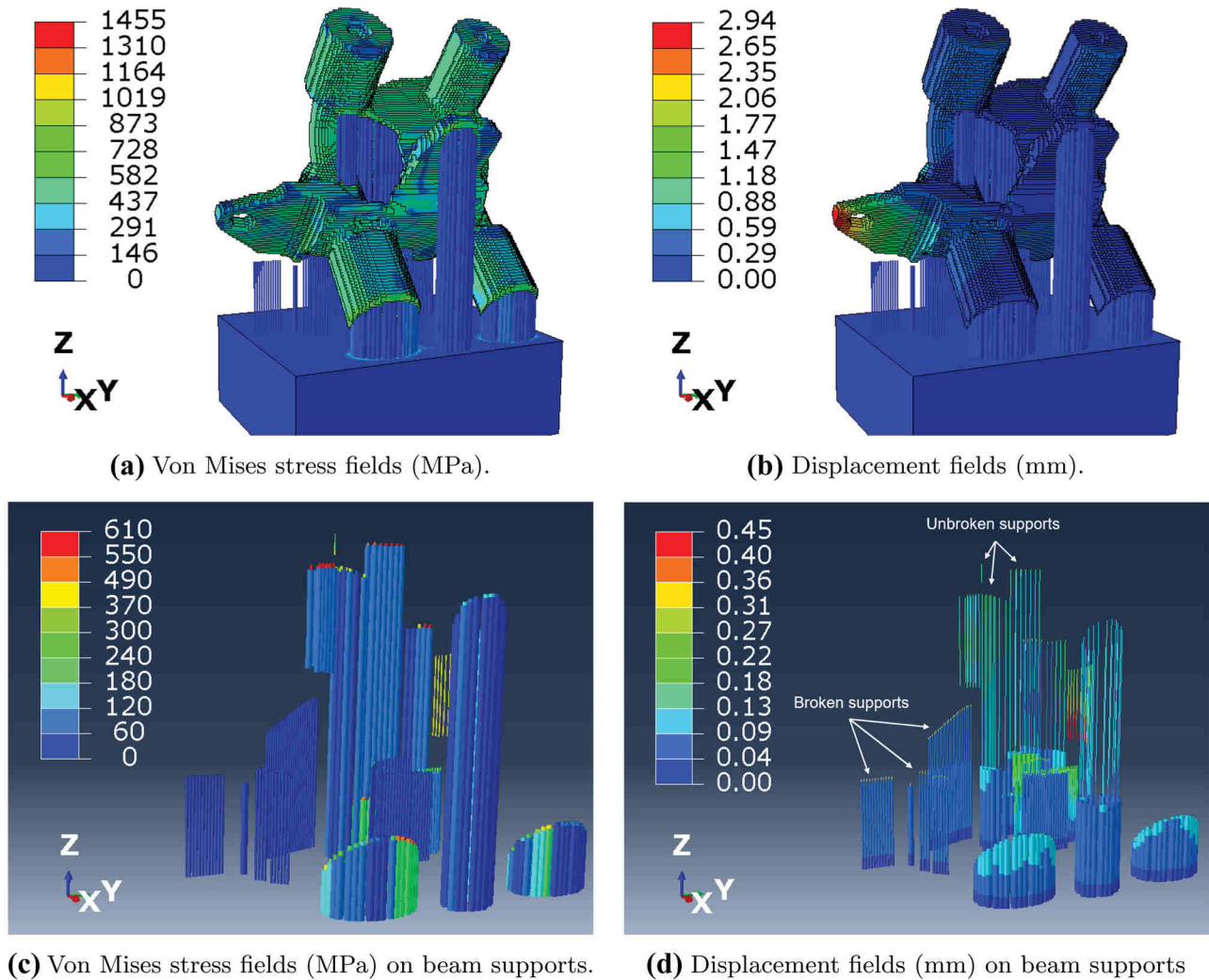
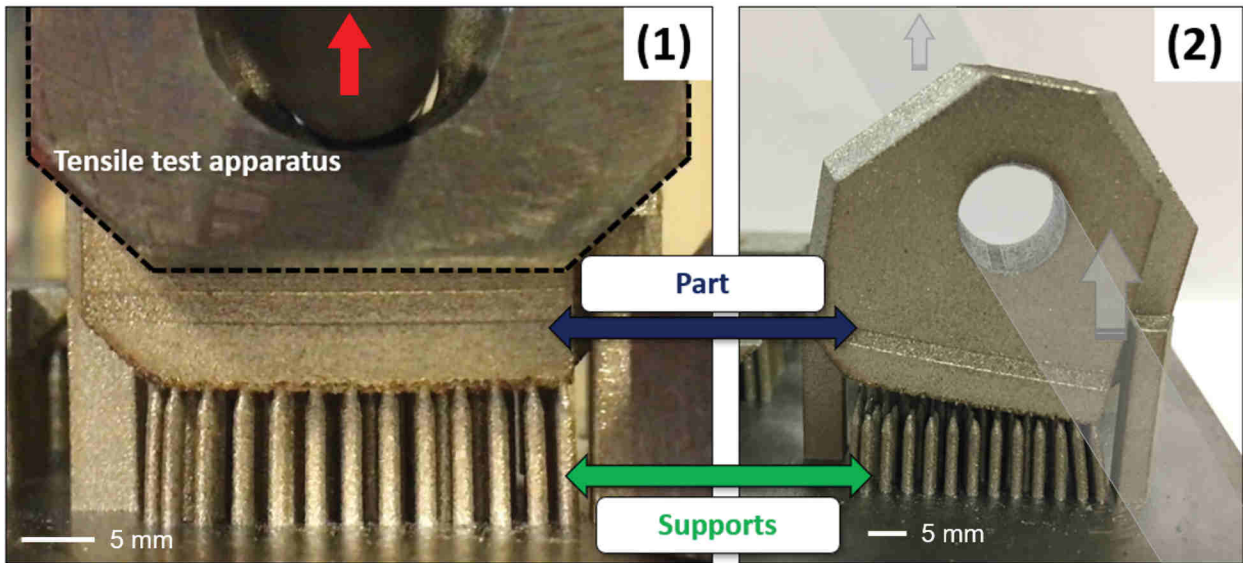


Fig. 9 Beam elements simulation results: stress and displacement fields

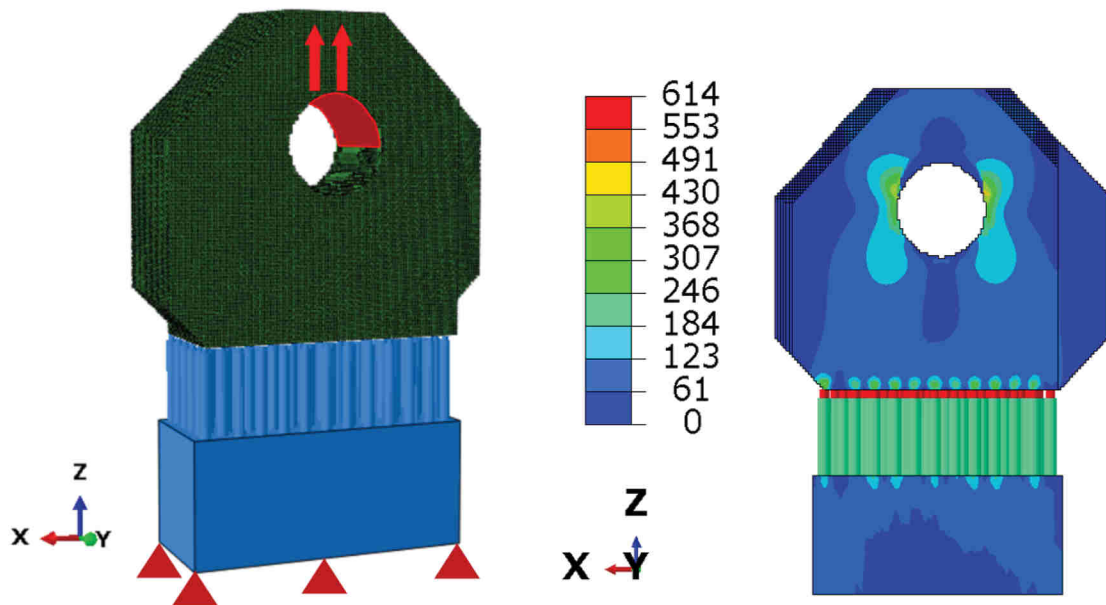
from 1.10 mm to 0.75 mm is abrupt, and a smoother variation might be implemented using non-standard beam elements in a future work. As in the hydraulic joint case, the value 0.75 mm was proposed as standard by the manufacturer software. The mesh size applied to the supports was 0.1 mm in order to accurately retrieve the force magnitude and the displacement fields. Supports were meshed using 5 530 linear B31 beam elements. The set up consisted of a part that could be pulled from a central hole. The contact at the central hole was idealised through the superior surface of the hole, this assumption having no impact on the teeth loadings. The numerical model was established with the same file used for the production. The part was meshed using 305 434 linear hexahedral elements of type C3D8I (mesh size of 250 μm). A reduced build plate of dimensions 22.5 mm * 10 mm * 9.3 mm was used to numerically attach the supports. The boundary condition applied at the bottom of the build plate prevented any displacements. As in

the hydraulic joint model, the beams rotations were artificially frozen to avoid instabilities due to multiple buckling. A vertical displacement boundary condition of 0.7 mm was set at the hole's upper surface to simulate the experimental loading. Taking into account the elasticity of the mounting assembly (the *Tensile test apparatus* on Fig. 10a) in a specific numerical model. It was concluded that the mounting assembly elasticity did not have a significant influence on the tensile results, hence it could be assimilated as an rigid assembly.

The multi-supports set up model and simulation at a specific displacement increment (for which the peak stress value is attained) are displayed on Fig. 10. From Fig. 10c, it could be seen that the main stresses are located at the tooth area. The underlying supports having a larger diameter (1.10 mm compared to 0.75 mm at the tooth location) suffer less than half the stress magnitude than the teeth. The extracted displacements were chosen at the top of a tooth



(a) Experimental multi-supports set-up: (1) During loading, dashed lines delimit the tensile test apparatus tied to the part. (2) After supports detachment and unloading, all breakages were located at the teeth. Grey areas and arrows show the position of the rod and the pulling direction.



(b) Abaqus model of the multi-support set-up. (c) Von Mises stress fields at the peak stress value.

Fig. 10 Multiple cone supports experimental and model set-up, as well as simulation results at the peak stress value

(the displacement was similar for all teeth). The reaction forces were retrieved from the bottom surface of the build plate (as in Fig. 10a).

The whole force-strain curves from the experimental tensile test and the simulation are shown on Fig. 11. The simulated curves are shown with two different values of the effective plastic displacement at the point of failure, presented

in Section 4.1. It could be seen that the better match of the completed damage is obtained using the value 0.01 for the effective plastic displacement at the point of failure.

In the hydraulic joint model (Section 4.2), the 0.05 parameter value was used. Indeed, it was not possible for the simulation to converge while using a most suitable effective plastic displacement parameter (0.01). Hence, while using a

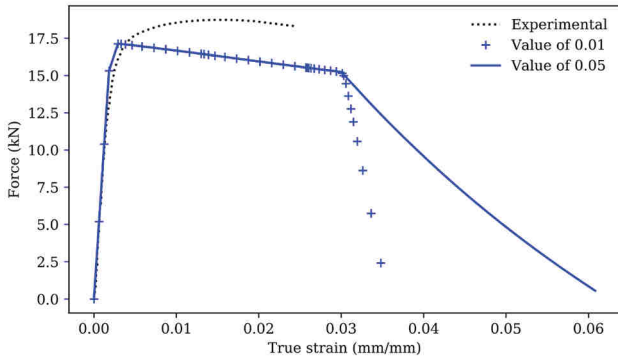


Fig. 11 Multi-supports set up experimental and simulated force-strain tensile test result

value of 0.05, 126 supports were detached from the hydraulic joint model. Using the degradation variable, it was possible to estimate the number of additional detached supports with a value of 0.01: only 7 more would have been detached. Then, increasing the number of supports increases the risk of having several damaged supports, and the risk for the simulations to fail to converge.

It can be observed in Fig. 11 that the simulated plastic behaviour is below the experimental. This shows that the tensile strength value that was set in the model (614 MPa) is too low. Hence, the global elasto-plastic behaviour of the cone supports needs to be further characterised.

The difference between the maximum force of the simulated test (17.1 kN) and the experimental one (18.7 kN) were about 8.5%. Hence, the behaviour of the modelled supports taken together as a group is considered similar to the experimental. In the next section, the individual supports mechanical response is considered under tensile loading.

4.2.3 Single beam mechanical testing

In the previous section, several supports were considered as a whole (numerous identical supports of the same height and diameter, all connected to the same part surface). Seventy-nine supports together were tested using a specific experimental set up. In this section, the behaviour of an individual cone supports will be looked upon.

It is assumed that the mechanical characteristics of the manufactured cone supports may differ greatly from the bulk part's because of their specific thermal history. In particular, cone supports are surrounded by thermally insulating powder particles, causing the heat to be mostly diffused in the vertical direction. The thermal history difference between the cone supports and the part could lead to specific microstructures or even defects (i.e. porosity). Hence, the literature mechanical characteristics listed in Table 4 may not be

suitable to the supports. In order to perform tensile tests on individual supports, i.e. a bar with a small diameter, another specific set up was designed, as can be seen in Fig. 12.

The tensile tests were performed on an Instron Electropulse 3kN apparatus, and the distortion was measured using mechanical extensometry with an 2620-604 Instron extensometer. A specific set up was manufactured in three parts and assembled as shown in Fig. 12. The support has a uniform diameter of 0.95 mm (supports with diameters below this limit show manufacturing issues when built with great heights). It has a total height of 33 mm and an operating length (outside the clamping) of 23 mm. A 5 mm lid was designed at the support edges for the assembly within the clamping. The resulting tensile test curves for nine individual supports are displayed in Fig. 13. It can be seen from the stress-strain curves that the results are homogeneous between the cone supports. Regarding the mechanical properties, the mean Young modulus was about 106 GPa (instead of 180 GPa from literature values, see Table 4). The yield strength was about 400 MPa (instead of 496 MPa) and the tensile strength is estimated at 520 MPa (instead of 614 MPa). Thus, it can be concluded that the material properties assigned to the part differ significantly from individual cone supports'. It is worth mentioning that only one support broke below a strain of 30%, and the other ones broke at a strain above 35% (the maximum measured fracture strain being 48%). Single beam tensile results were used in the numerical design of experiment to test the supports mechanical sensibility (Case 3 in Table 5). The fracture strain assigned within the simulations was set to 34%.

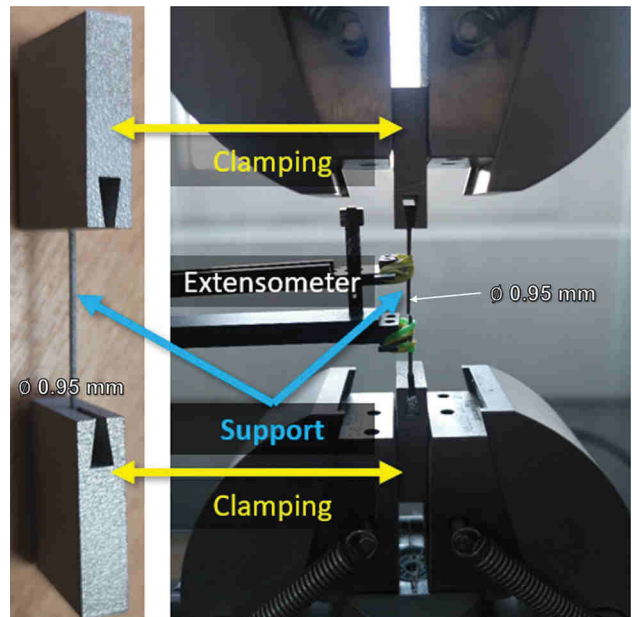


Fig. 12 Individual support set up (left) and inside the tensile test apparatus with the extensometer (right)

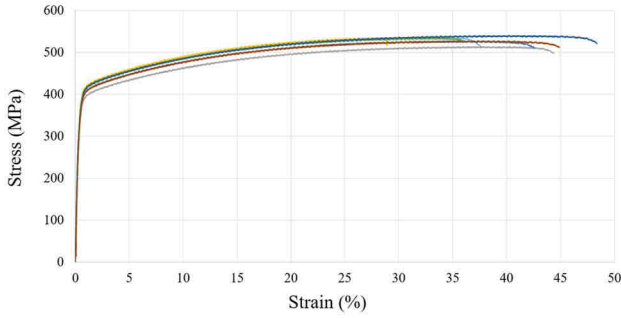


Fig. 13 Individual beam support tensile test stress-strain results

Hence, in the following section, specific support mechanical properties will be assigned within the hydraulic joint model and several scenarios compared. The objective of these two sections is to compare the number of broken supports by the end of the simulation and identify the key parameters. A complementary objective would be to fully characterise the mechanical behaviour of the support teeth. At the moment, these ranges of diameters (below 0.9 mm) are difficult to manufacture by SLM on a sufficient height. These experimental teeth characterisation will be the topic of a future study.

4.2.4 Beam supports mechanical sensibility

In the previous section, individual support tensile tests have been performed, showing that the bulk part mechanical properties differ significantly from the supports'. In the current section, two separate study cases are performed to understand the key parameters to be assigned to the modelled supports. The first case is the reference, for which the simulation results have already been analysed (Section 4.2). For this first study case, the bulk material characteristics found in the literature have been assigned to the supports. The second case "Case 2" has a higher fracture strain parameter than the reference case: the fracture strain is set at 45% instead of 34%. All the other parameters are equal to those of the reference case. The third case "Case 3" has equal fracture strain to the reference case (34%), but its elasto-plastic properties are lowered: Young Modulus is set at 106 GPa, the

Table 5 Mechanical properties and the number of broken supports for the different cone support sensibility cases

Characteristics	Ref.	Case 2	Case 3
Young Modulus E (GPa)	180	180	106
Yield strength R_e (MPa)	496	496	400
Tensile strength R_m (MPa)	614	614	520
Fracture strain $A\%$ (%)	34	45	34
Broken supports / Exp	126/12	105/12	125/12

yield and tensile strengths are set at 400 MPa and 520 MPa respectively. The changes are driven by the experimental results of the individual cone supports (Fig. 13). Table 5 lists the different study cases parameters.

While using weakened mechanical properties for the supports (Case 3), and keeping the same fracture strain (34%), the number of broken supports remained the same (125 instead of 126 in Reference case, Section 4.2). On the contrary, while keeping the same elasto-plastic properties as the part's, and providing a greater fracture strain (45% instead of 34%, Case 2), the number of broken supports diminishes to 105. Hence, the fracture strain could be considered as one of the key parameters to precisely characterise in order to simulate the supports breakage.

Considering the three material characteristics cases (see Table 5) and the number of broken supports, it can be concluded that assigning greater fracture strain parameter improves fairly the simulation results.

5 Conclusions and perspectives

The Selective Laser Melting process is one of the most studied additive manufacturing processes both in the industry and academic research fields. A significant challenge of this process is anticipating the various flaws while manufacturing the parts, including the distortions and fractures. While using numerous supports for anchoring the part, some may be damaged and even detached without invalidating the part. Simulating the supports' damage and being able to track the ongoing deflection was the scope of this paper.

An industrial part was chosen as a study case. Its manufacturing completed, but some supports have broken, making the part warp and slightly collide with the layering system. Four commercial software were firstly used to simulate the manufacturing process, and all the results show a significant distortion of the part. However, none of these codes was able to predict supports breakage. The Abaqus developed models in this article are intended to model the overall distortion, damage and cracking of cone supports.

All the developed models considered were strictly quasi-static mechanical. And, for sake of simplicity, loads were assigned as user-defined temperature increments along the activated macro layers. However, full thermal modelling could be considered. Two types of models were developed to mesh the supports: 3D voxel elements and 1D-beam elements. Only the 1D-beam elements could easily incorporate the shrinkage in the teeth section. To approximate the shrinkage in the voxels model, a local change in the material properties would have been necessary. However, identifying the location of the specific shrinkage material properties in the voxels model could be delicate to perform using a global STL file containing both the supports and the part.

While using 1D-beam elements to mesh the cone supports, a whole supported region was detached. However, no fracture was observed in the voxel elements model. The difference between voxel and 1D-beam elements could be explained by the absence of geometrical narrowing corresponding to the teeth while using voxel elements.

Experimental tensile tests using specific set-ups have been performed to compare a group of supports as a whole, which guarantee a realistic thermal history. An other set-up has been done for a unique cone support also, thus less thermally realistic but allowing a finer analysis. Regarding the group of supports, it was observed that the difference in the maximum force applied was below 10%. However, the plastic behaviour did not follow the experiment and it seems necessary to characterise it more accurately in the future. Then, the individual cone support behaviour was characterised since it is assumed that the specific thermal history of the supports influence the microstructure and consequently, the mechanical behaviour. The fracture strain may be slightly greater, but the Young modulus and the strengths are weaker. It has been shown that the supports mechanical properties differ significantly from the bulk parts.

Regarding the hydraulic joint 1D-beam elements simulation, too many supports have been detached from the part during the simulation (126 instead of 12, experimentally). Various modelling simplifications (such as the user-defined thermal variations, from the melting temperature to the room-ambient temperature) may explain this discrepancy. However, a potential improvement solution resides in precisely characterising the fracture strain parameter. Indeed, using a value of 45% (instead of 34%) led to a decrease of the number of detached supports down to 21. Also, the mechanical characterisation of teeth could reveal very instructive since the teeth constitute the fracture site in every case (experimental and simulated). For now, it is technically challenging to manufacture SLM isolated supports with the teeth diameter. Hence, this work will be the focus of a complementary study.

It was noticed that with an increasing number of cone supports, it could reveal more and more challenging to find suitable damage evolution parameters and boundary conditions allowing the simulations to complete. It is expected that running a simulation comprising several parts, each of these having hundreds of cone supports (as in our study case), would make a global convergence inaccessible because of the numerous supports cracking. A possible solution to tackle these convergence issues would be to use equivalent homogeneous materials to approximate the support structures. The elasto-plastic and damage behaviour of these equivalent materials would have to be finely tuned to follow the sensitive support behaviour.

Author contributions Partial financial support was received from Halbronn company (salary of the PhD, CIFRE, and financial contract with the laboratory, with the funding of the French funding agency ANRT).

Funding information **Y. Bresson**: Software, Methodology, Writing-Original draft preparation. **A. Tongne**: Software, Methodology, Writing-Reviewing and Editing. **P. Selva**: Experiments, Methodology, Writing-Reviewing and Editing. **L. Arnaud**: Supervision, Methodology, Writing-Reviewing and Editing.

Availability of data and materials Data and materials are available upon specific request.

Declarations

Conflict of interest The authors have no conflicts of interest to declare that are relevant to the content of this article.

References

1. ISO/TC (2018) PR NF EN ISO/ASTM 52911-1:2018-01 Additive manufacturing - Technical design guideline for powder bed fusion - Part 1: Laser-based powder bed fusion of metals
2. Gan MX, Wong CH (2016) Practical support structures for selective laser melting. *J Mater Process Technol* 238:474–484. <https://doi.org/10.1016/j.jmatprotec.2016.08.006>
3. Jiang J, Xu X, Stringer J (2018) Support Structures for Additive Manufacturing: A Review. *J Manu Mater Process* 2(4):64. <https://doi.org/10.3390/jmmp2040064>
4. Flores I, Kretzschmar N, Hadi A, Chekurov S, Bue D, Chaudhuri A (2020) Implications of lattice structures on economics and productivity of metal powder bed fusion. *Additive Manufacturing* 31(November 2019):100947. <https://doi.org/10.1016/j.addma.2019.100947>
5. (2020) VELO3D Website. <https://www.velo3d.com/>
6. Das P, Chandran R, Samant R, Anand S (2015) Optimum Part Build Orientation in Additive Manufacturing for Minimizing Part Errors and Support Structures. In: *Procedia Manufacturing*, Elsevier B.V., vol 1, pp 343–354. <https://doi.org/10.1016/j.promfg.2015.09.041>
7. Zhang K, Fu G, Zhang P, Ma Z, Mao Z, Zhang DZ (2018) Study on the geometric design of supports for overhanging structures fabricated by selective laser melting. *Materials* 12(27):1–16. <https://doi.org/10.3390/ma12010027>
8. Cao Q, Shi Z, Bai Y, Zhang J, Zhao C, Fuh JYH, Wang H (2021) A novel method to improve the removability of cone support structures in selective laser melting of 316L stainless steel. *J Alloys Comp* 854:1571332020.157133. <https://doi.org/10.1016/j.jallcom.2020.157133>
9. Hildreth OJ, Nassar AR, Chasse KR, Simpson TW (2016) Dissolvable metal supports for 3D direct metal printing. *3D Printing and Additive Manufacturing* 3(2):91–97. <https://doi.org/10.1089/3dp.2016.0013>
10. Lefky CS, Zucker B, Wright D, Nassar AR, Simpson TW, Hildreth OJ (2017) Dissolvable Supports in Powder Bed Fusion-Printed Stainless Steel. *3D Printing and Additive Manufacturing* 4(1):3–11. <https://doi.org/10.1089/3dp.2016.0043>
11. Mumtaz K, Vora P, Hopkinson N (2011) A method to eliminate anchors supports from directly laser melted metal powder bed processes. In: *Proceedings of the Solid Freeform Fabrication Symposium*, Austin, Texas, pp 55–64. <https://doi.org/10.16194/j.cnki.31-1059/g4.2011.07.016>

12. Raikar S, Heilig M, Mamidanna A, Hildreth OJ (2021) Self-terminating etching process for automated support removal and surface finishing of additively manufactured Ti-6Al-4V. *Additive Manufacturing* 37(June 2020):101694. <https://doi.org/10.1016/j.addma.2020.101694>
13. Calignano F (2014) Design optimization of supports for overhanging structures in aluminum and titanium alloys by selective laser melting. *Mater Des* 64:203–213. <https://doi.org/10.1016/j.matdes.2014.07.043>
14. Thomas D (2012) The Development of Design Rules for Selective Laser Melting. PhD thesis, University of Wales Institute, Cardiff. <http://www.fhrcr.org>
15. Leary M, Maconachie T, Sarker A, Faruque O, Brandt M (2019) Mechanical and thermal characterisation of AlSi10Mg SLM block support structures. *Mater Des* 183. <https://doi.org/10.1016/j.matdes.2019.108138>
16. Bobbio LD, Qin S, Dunbar A, Michaleris P, Beese AM (2017) Characterization of the strength of support structures used in powder bed fusion additive manufacturing of Ti-6Al-4V. *Addit Manuf* 14:60–68. <https://doi.org/10.1016/j.addma.2017.01.002>
17. Zeng K (2015) Optimization of support structures for selective laser melting. PhD thesis, University of Louisville, <https://doi.org/10.18297/etd/2221>
18. (2020) Altair Inspire Print3D Website. <https://solidthinking.com/product/inspire-print3d/>
19. (2020) © Additive Works GmbH Website. <https://additive.works/overview>
20. (2020) Netfabb® Website. <https://www.autodesk.fr/products/netfabb>
21. (2020) Simufact Additive Website. <https://www.simufact.com/simufact-additive.html>
22. (2018) ESI Group Website. <https://www.esi-group.com/software-solutions/virtual-manufacturing/additive-manufacturing>
23. Ganeriwala RK, Hodge NE, Solberg JM (2021) Towards improved speed and accuracy of laser powder bed fusion simulations via multiscale spatial representations. *Computational Materials Science* 187(November 2020):110112. <https://doi.org/10.1016/j.commatsci.2020.110112>
24. Li C, Fu C, Guo Y, Fang F (2016) A multiscale modeling approach for fast prediction of part distortion in selective laser melting. *J Mat Proc Tech* 229:703–712. <https://doi.org/10.1016/j.jmatprotec.2015.10.022>
25. Markl M, Körner C (2016) Multiscale Modeling of Powder Bed-Based Additive Manufacturing. *Annual Rev Mat Res* 46(1):93–123. <https://doi.org/10.1146/annurev-matsci-070115-032158>
26. Mercelis P, Kruth JP (2006) Residual stresses in selective laser sintering and selective laser melting. *Rapid Prototyp J* 12(5):254–265. <https://doi.org/10.1108/13552540610707013>
27. Mukherjee T, Zuback JS, De A, DebRoy T (2016) Printability of alloys for additive manufacturing. *Sci Rep* 6:1–8. <https://doi.org/10.1038/srep19717>
28. Mukherjee T, Manvatkar V, De A, DebRoy T (2017) Mitigation of thermal distortion during additive manufacturing. *Scripta Mater* 127:79–83. <https://doi.org/10.1016/j.scriptamat.2016.09.001>
29. Hooper PA (2018) Melt pool temperature and cooling rates in laser powder bed fusion. *Addit Manuf* 22(May):548–559. <https://doi.org/10.1016/j.addma.2018.05.032>
30. Denlinger ER, Michaleris P (2016) Effect of stress relaxation on distortion in additive manufacturing process modeling. *Addit Manuf* 12:51–59. <https://doi.org/10.1016/j.addma.2016.06.011>
31. Ganeriwala R, Strantzsa M, King W, Clausen B, Phan T, Levine L, Brown D, Hodge N (2019) Evaluation of a thermomechanical model for prediction of residual stress during laser powder bed fusion of Ti-6Al-4V. *Addit Manuf* 27(April):489–502. <https://doi.org/10.1016/j.addma.2019.03.034>
32. Mukherjee T, Zhang W, DebRoy T (2017) An improved prediction of residual stresses and distortion in additive manufacturing. *Comput Mater Sci* 126:360–372. <https://doi.org/10.1016/j.commatsci.2016.10.003>
33. Parry L, Ashcroft IA, Wildman RD (2016) Understanding the effect of laser scan strategy on residual stress in selective laser melting through thermo-mechanical simulation. *Addit Manuf* 12:1–15. <https://doi.org/10.1016/j.addma.2016.05.014>
34. Paul R, Anand S, Gerner F (2014) Effect of Thermal Deformation on Part Errors in Metal Powder Based Additive Manufacturing Processes. *J Manuf Sci Eng* 136(3). <https://doi.org/10.1115/1.4026524>
35. Zaeh MF, Branner G (2010) Investigations on residual stresses and deformations in selective laser melting. *Prod Eng Res Devel* 4(1):35–45. <https://doi.org/10.1007/s11740-009-0192-y>
36. Lindgren LE, Runnemalm H, Näsström MO (1999) Simulation of multipass welding of a thick plate. *Int J Numer Meth Eng* 44(9):1301–1316. [https://doi.org/10.1002/\(SICI\)1097-0207\(19990330\)44:9<1301::AID-NME479>3.0.CO;2-K](https://doi.org/10.1002/(SICI)1097-0207(19990330)44:9<1301::AID-NME479>3.0.CO;2-K)
37. Michaleris P (2014) Modeling metal deposition in heat transfer analyses of additive manufacturing processes. *Finite Elem Anal Des* 86:51–60. <https://doi.org/10.1016/j.finela.2014.04.003>
38. Li C, Liu ZY, Fang XY, Guo YB (2018) On the Simulation Scalability of Predicting Residual Stress and Distortion in Selective Laser Melting. *J Manuf Sci Eng* 140(4). <https://doi.org/10.1115/1.4038893>
39. Ueda Y, Fukuda K, Tanigawa M (1979) New Measuring Method of Three Dimensional Residual Stresses Based on Theory of Inherent Strain(Welding Mechanics, Strength & Design). *Trans JWRI* 8(2):249–256
40. Bugatti M, Semeraro Q (2018) Limitations of the inherent strain method in simulating powder bed fusion processes. *Addit Manuf* 23(May):329–346. <https://doi.org/10.1016/j.addma.2018.05.041>
41. Keller N (2016) Nils Keller verfahren durch Multi-Skalen-Simulation Verzugsminimierung bei selektiven Laserschmelzverfahren durch. PhD thesis, Universität Bremen
42. Keller N, Ploshikhin V (2014) New method for fast predictions of residual stress and distortion of AM parts. In: *Solid Freeform Fabrication*, pp 1689–1699. <https://doi.org/10.1017/CBO9781107415324.004>
43. Liang X, Cheng L, Chen Q, Yang Q, To AC (2018) A modified method for estimating inherent strains from detailed process simulation for fast residual distortion prediction of single-walled structures fabricated by directed energy deposition. *Addit Manuf* 23(August):471–486. <https://doi.org/10.1016/j.addma.2018.08.029>
44. Siewert M, Neugebauer F, Epp J, Ploshikhin V (2019) Validation of Mechanical Layer Equivalent Method for simulation of residual stresses in additive manufactured components. *Comput Math Appl* 78(7):2407–2416. <https://doi.org/10.1016/j.camwa.2018.08.016>
45. Bartsch K, Lange F, Gralow M, Emmelmann C (2019) Novel approach to optimized support structures in laser beam melting by combining process simulation with topology optimization. *J Laser Appl* 31(2):022302, 1–7. <https://doi.org/10.2351/1.5096096>
46. Liang X, Dong W, Hinnebusch S, Chen Q, Tran HT, Lemon J, Cheng L, Zhou Z, Hayduke D, To AC (2020) Inherent strain homogenization for fast residual deformation simulation of thin-walled lattice support structures built by laser powder bed fusion additive manufacturing. *Additive Manufacturing* 32(October 2019):101091. <https://doi.org/10.1016/j.addma.2020.101091>
47. Tran HT, Chen Q, Mohan J, To AC (2020) A new method for predicting cracking at the interface between solid and lattice support during laser powder bed fusion additive manufacturing. *Addit Manuf* 32(January). <https://doi.org/10.1016/j.addma.2020.101050>

48. Zhang ZD, Ibadode O, Ali U, Dibia CF, Rahnama P, Bonakdar A, Toyserkani E (2020) Topology optimization parallel-computing framework based on the inherent strain method for support structure design in laser powder-bed fusion additive manufacturing. *Int J Mech Mat Des* 0123456789. <https://doi.org/10.1007/s10999-020-09494-x>
49. Järvinen JP, Matilainen V, Li X, Piili H, Salminen A, Mäkelä I, Nyrhilä O (2014) Characterization of effect of support structures in laser additive manufacturing of stainless steel. *Physics Procedia* 56(C):72–81. <https://doi.org/10.1016/j.phpro.2014.08.099>
50. Cao Q, Bai Y, Zhang J, Shi Z, Fuh JYH, Wang H (2020) Removability of 316L stainless steel cone and block support structures fabricated by Selective Laser Melting (SLM). *Mater Des* 191. <https://doi.org/10.1016/j.matdes.2020.108691>
51. Weber S, Montero J, Petroll C, Schäfer T, Bleckmann M, Paetzold K (2020) The Fracture Behavior and Mechanical Properties of a Support Structure for Additive Manufacturing of Ti-6Al-4V. *Curr Comput-Aided Drug Des* 10(5):343. <https://doi.org/10.3390/cryst10050343>
52. Ainsworth I, Rayner GD, McClelland MJ, Revanur R, Ferrar BI (2016) US20160306901A1. Improvements in or relating to the building of supports in additive manufacturing. <https://patents.google.com/patent/US20160306901A1/en>
53. Burhop MR, Madeley D, Musuvathy S, Arisoy E, Slavin E, Bank H (2017) US9844917B2 Support structures for additive manufacturing of solid models. <https://patents.google.com/patent/US9844917B2/en>
54. Wang Z, Zhang Y, Tan S, Ding L, Bernard A (2021) Support point determination for support structure design in additive manufacturing. *Additive Manufacturing* 47(August):102341, 10.1016/j.addma.2021.102341, <https://doi.org/10.1016/j.addma.2021.102341>
55. Barth FM (2018) US20180304541A1. 3D Lattice supports for additive manufacturing. <https://patents.google.com/patent/US20180304541A1/en>
56. Fieldman Z (2017) US10744713B2. Methods and breakable supports for additive manufacturing. <https://patents.google.com/patent/US10744713B2/en>
57. Fieldman Z, Hall C (2018) US20180141122A1. Methods and spoke supports for additive manufacturing. <https://patents.google.com/patent/US20180141122A1/en>
58. Fieldman Z, Joerger D, Dunham N (2019a) US10391753B2. Methods and keyway supports for additive manufacturing. <https://patents.google.com/patent/US10391753B2/en>
59. Fieldman Z, Sinnett T, Joerger D, Dunham N (2019b) US10357828B2. Methods and leading edge supports for additive manufacturing. <https://patents.google.com/patent/US10357828B2/en>
60. Joerger D (2017) US10799951B2. Method and conformal supports for additive manufacturing. <https://patents.google.com/patent/US10799951B2/en>
61. Joerger D, Dunham N (2020) US10583606B2. Method and supports with powder removal ports for additive manufacturing. <https://patents.google.com/patent/US10583606B2/en>
62. Marte E, Fieldman Z, Sinnett T, Joerger D, Dunham N, Miller M (2020) US10549478B2. Methods and surrounding supports for additive manufacturing. <https://patents.google.com/patent/US10549478B2/en>
63. Marte EMA, Sinnett T, Joerger D, Dunham N (2019) US10486362B2. Method and connecting supports for additive manufacturing. <https://patents.google.com/patent/US10486362B2/en>
64. Stoyanov P (2018) US9975182B2. Cutting Tool Made by Additive Manufacturing. <https://patents.google.com/patent/US9975182B2/en>
65. Van Espen J (2018) US10843412B2. Support structures in additive manufacturing. <https://patents.google.com/patent/US10843412B2/en>
66. Gold SA, Kenney PM (2018) US20180029306A1. Methods using ghost supports for additive manufacturing. <https://patents.google.com/patent/US20180029306A1/en>
67. Ploshikhin V (2018) DE102017113485A1. Method for the additive production of at least one component, support structure or element of a support structure, component with the same and installation for carrying out such a method. <https://patents.google.com/patent/DE102017113485A1/en?inventor=ploshikhin&before=priority:20210101&after=priority:20170101>
68. Cloots M, Spierings A, Wegener K (2013) Assessing new support minimizing strategies for the additive manufacturing technology SLM. In: *Solid freeform fabrication symposium*, pp 631–643
69. Jhabvala J, Boillat E, André C, Glardon R (2012) An innovative method to build support structures with a pulsed laser in the selective laser melting process. *Int J Adv Manuf Technol* 59(1–4):137–142. <https://doi.org/10.1007/s00170-011-3470-8>
70. Paul R, Anand S (2015) Optimization of layered manufacturing process for reducing form errors with minimal support structures. *J Manuf Syst* 36:231–243. <https://doi.org/10.1016/j.jmsy.2014.06.014>
71. Strano G, Hao L, Everson RM, Evans KE (2013) A new approach to the design and optimisation of support structures in additive manufacturing. *Int J Adv Manuf Technol* 66(9–12):1247–1254. <https://doi.org/10.1007/s00170-012-4403-x>
72. Allaire G, Bogosel B (2018) Optimizing supports for additive manufacturing. HAL
73. Song J, Chew Y, Yao X, Jiao L, Bi G, Moon SK (2018) Numerical study of temperature and cooling rate in selective laser melting with functionally graded support structures. *Addit Manuf* 24(August):543–551. <https://doi.org/10.1016/j.addma.2018.10.039>
74. Zhou M, Liu Y, Lin Z (2019) Topology optimization of thermal conductive support structures for laser additive manufacturing. *Comput Methods Appl Mech Eng* 353:24–43. <https://doi.org/10.1016/j.cma.2019.03.054>
75. Kajima Y, Takaichi A, Nakamoto T, Kimura T, Kittikundecha N, Tsutsumi Y, Nomura N, Kawasaki A, Takahashi H, Hanawa T (2017) Wakabayashi N (2018) Effect of adding support structures for overhanging part on fatigue strength in selective laser melting. *J Mech Behav Biomed Mater* 78:1–9. <https://doi.org/10.1016/j.jmbbm.2017.11.009>
76. Poyraz Ö, Yasa E, Akbulut G, Orhangül A, Pilatin S (2015) Investigation of support structures for direct metal laser sintering (DMLS) of IN625 parts. *Solid Freeform Fabrication (SFF) Symposium*. Austin, Texas, pp 560–574
77. Cheng L, Liang X, Bai J, Chen Q, Lemon J (2018) To A (2019) On Utilizing Topology Optimization to Design Support Structure to Prevent Residual Stress Induced Build Failure in Laser Powder Bed Metal Additive Manufacturing. *Addit Manuf* 27:290–304. <https://doi.org/10.1016/j.addma.2019.03.001>
78. Krol TA, Zaeh MF, Seidel C (2012) Optimization of supports in metal-based additive manufacturing by means of finite element models. *23rd Annual International Solid Freeform Fabrication Symposium - An Additive Manufacturing Conference, SFF 2012*. Austin, Texas, pp 707–718
79. Mele M, Bergmann A, Campana G, Pilz T (2021) Experimental investigation into the effect of supports and overhangs on accuracy and roughness in laser powder bed fusion. *Optics and Laser Technology* 140(November 2020). <https://doi.org/10.1016/j.optlastec.2021.107024>
80. Benoist V, Arnaud L, Baili M, Faye P (2018) Topological optimization design for additive manufacturing, taking into account flexion and vibrations during machining post processing operations. In: *14Th International Conference on High Speed Machining, San Sebastian, Spain*, pp 1–4, <https://hal.archives-ouvertes.fr/hal-01905429>

81. Renishaw (2020) SS 316L-0407 powder for additive manufacturing. <https://www.renishaw.com/en/data-sheets-additive-manufacturing--17862>
82. Outokumpu (2013) Handbook of stainless steel. Tech. rep
83. Ahmadi A, Mirzaeifar R, Moghaddam NS, Turabi AS, Karaca HE, Elahinia M (2016) Effect of manufacturing parameters on mechanical properties of 316L stainless steel parts fabricated by selective laser melting: A computational framework. *Mater Des* 112:328–338. <https://doi.org/10.1016/j.matdes.2016.09.043>
84. Alsalla H, Hao L, Smith C (2016) Effect of build orientation on the surface quality, microstructure and mechanical properties of selective laser melting 316L stainless steel. *Rapid Prototyp J*
85. Casati R, Lemke J, Vedani M (2016) Microstructure and Fracture Behavior of 316L Austenitic Stainless Steel Produced by Selective Laser Melting. *J Mater Sci Technol* 32(8):738–744. <https://doi.org/10.1016/j.jmst.2016.06.016>
86. Chen W, Yin G, Feng Z, Liao X (2018) Effect of Powder Feedstock on Microstructure and Mechanical Properties of the 316L Stainless Steel Fabricated by Selective Laser Melting. *Metals* 8(9):729. <https://doi.org/10.3390/met8090729>
87. Heiden MJ, Deibler LA, Rodelas JM, Koepke JR, Tung DJ, Saiz DJ (2018) Jared BH (2019) Evolution of 316L stainless steel feedstock due to laser powder bed fusion process. *Addit Manuf* 25:84–103. <https://doi.org/10.1016/j.addma.2018.10.019>
88. Mertens A, Reginster S, Contrepois Q, Dormal T, Lemaire O, Lecomte-Beckers J (2014) Microstructures and mechanical properties of stainless steel aisi 316l processed by selective laser melting. *Mater Sci Forum* 783–786:898–903. <https://doi.org/10.4028/www.scientific.net/msf.783-786.898>
89. Röttger A, Boes J, Theisen W, Thiele M, Esen C, Edelmann A, Hellmann R (2020) Microstructure and mechanical properties of 316L austenitic stainless steel processed by different SLM devices. *Int J Adv Manuf Technol* 108(3):769–783. <https://doi.org/10.1007/s00170-020-05371-1>
90. Shamsujjoha M, Agnew SR, Fitz-Gerald JM, Moore WR, Newman TA (2018) High Strength and Ductility of Additively Manufactured 316L Stainless Steel Explained. *Metall Mater Trans A* 49(7):3011–3027. <https://doi.org/10.1007/s11661-018-4607-2>
91. Stoll P, Spierings A, Wegener K (2019) Impact of a process interruption on tensile properties of SS 316L parts and hybrid parts produced with selective laser melting. *Int J Adv Manuf Technol* 103(1–4):367–376. <https://doi.org/10.1007/s00170-019-03560-1>
92. Suryawanshi J, Prashanth KG, Ramamurty U (2017) Mechanical behavior of selective laser melted 316L stainless steel. *Mater Sci Eng, A* 696(April):113–121. <https://doi.org/10.1016/j.msea.2017.04.058>
93. Tolosa I, Garciandía F, Zubiri F, Zapirain F, Esnaola A (2010) Study of mechanical properties of AISI 316 stainless steel processed by selective laser melting, following different manufacturing strategies. *Int J Adv Manuf Tech* 51(5–8):639–647. <https://doi.org/10.1007/s00170-010-2631-5>
94. Wood P, Libura T, Kowalewski ZL, Williams G, Serjouei A (2019) Influences of Horizontal and Vertical Build Orientations and Post-Fabrication Processes on the Fatigue Behavior of Stainless Steel 316L Produced by Selective Laser Melting. *Materials* 12(4203):1–19
95. Zhong Y, Liu L, Wikman S, Cui D, Shen Z (2016) Intragranular cellular segregation network structure strengthening 316L stainless steel prepared by selective laser melting. *J Nucl Mater* 470:170–178. <https://doi.org/10.1016/j.jnucmat.2015.12.034>
96. ASTM International (1999) A666–15. Standard Specification for Annealed or Cold-Worked Austenitic Stainless Steel Sheet, Strip, Plate, and Flat Bar. <https://doi.org/10.1520/A0666-15.2>
97. Simulia (2014) Abaqus Analysis User's Manual 24.2.2 Damage initiation for ductile metals Products: Abaqus/Standard Abaqus/Explicit Abaqus/CAE. <http://130.149.89.49:2080/v6.8/books/usb/default.htm?startat=pt05ch20s02abm40.html>
98. Simulia (2015) Abaqus Analysis User's Manual 24.2.3 Damage evolution and element removal for ductile metals Products: Abaqus/Standard Abaqus/Explicit Abaqus/CAE. ABAQUS Manual pp 1–10, <https://classes.engineering.wustl.edu/2009/spring/mase5513/abaqus/docs/v6.6/books/usb/default.htm?startat=pt05ch18s02abm24.html>
99. Simulia (2006) Abaqus Getting Started with ABAQUS/Standard: Keywords Version 8.4 Example: connecting lug with plasticity. <https://classes.engineering.wustl.edu/2009/spring/mase5513/abaqus/docs/v6.6/books/gss/default.htm?startat=ch08s04.html>

Publisher's Note Springer Nature remains neutral with regard to jurisdictional claims in published maps and institutional affiliations.